

NEUROIMAGING

In vivo network models identify sex differences in the spread of tau pathology across the brain

Sepideh Shokouhi¹ | Warren D. Taylor^{1,2} | Kimberly Albert¹ | Hakmook Kang³ | Paul A. Newhouse^{1,2} | for The Alzheimer's Disease Neuroimaging Initiative

¹Center for Cognitive Medicine, Department of Psychiatry and Behavioral Sciences, Vanderbilt University Medical Center, Nashville, Tennessee

²Geriatric Research, Education, and Clinical Center, Tennessee Valley Veterans Affairs Medical Center, Nashville, Tennessee

³Department of Biostatistics, Vanderbilt University Medical Center, Nashville, Tennessee

Correspondence

Sepideh Shokouhi, PhD, Research Assistant Professor of Psychiatry and Behavioral Sciences, Center for Cognitive Medicine, Department of Psychiatry and Behavioral Sciences, Vanderbilt University Medical Center, 1601 23rd Avenue South, Nashville, TN 37212.
Email: sepideh.shokouhi@vanderbilt.edu

Funding information

National Institutes of Health, Grant/Award Numbers: R00EB009106, K24MH110598, R01AG047992

*Data used in preparation of this article were obtained from the Alzheimer's Disease Neuroimaging Initiative (ADNI) database (adni.loni.usc.edu). As such, the investigators within the ADNI contributed to the design and implementation of ADNI and/or provided data but did not participate in analysis or writing of this report. A complete listing of ADNI investigators can be found at: http://adni.loni.usc.edu/wp-content/uploads/how_to_apply/ADNI_Acknowledgement_List.pdf

Abstract

Introduction: We examined networks of tau connectivity between brain regions based on correlations of their [¹⁸F]flortaucipir positron emission tomography (PET) uptake to evaluate sex-specific differences in brain-wide tau propagation.

Methods: PET data of clinically normal and mild cognitive impairment (MCI) subjects from the Alzheimer's Disease Neuroimaging Initiative (ADNI) were used to examine differences in network architectures across the groups.

Results: The tau-based network architecture resembled progression of tauopathy from Braak stage I to VI regions. Compared to men, women had higher network density and an increased number of direct regional connections in co-occurrence with increased brain-wide tau burden, particularly at MCI. Several regions, including superior parietal lobe and parahippocampus served as connecting bridges between communities at different Braak stages.

Discussion: Network characteristics in women may favor an accelerated brain-wide tau spread leading to a higher tau burden in women than men with MCI with implications for the greater female preponderance in Alzheimer's disease diagnosis.

KEYWORDS

[¹⁸F]flortaucipir PET, Alzheimer's disease, mild cognitive impairment, network, sex differences, tau

1 | INTRODUCTION

Accumulating evidence suggests a prion-like spread of tauopathy,¹⁻⁵ which may drive the sequential involvement of affected regions that was first categorized at autopsy as Braak staging, ranging from stage I to stage VI.^{6,7} An increasing number of in vivo human imaging studies have demonstrated evidence of tau propagation through functionally (also possibly anatomically) connected regions.⁸⁻¹¹ Although the

prevalence of Alzheimer's disease (AD) is higher in women than in men,¹²⁻¹⁶ sex differences in tau spread are not fully understood. A recent study by Buckley and colleagues found that clinically normal amyloid beta-positive (A β +) women exhibited higher entorhinal cortical tau accumulation than men.¹⁷ In another study, Hohman and colleagues¹⁸ found a stronger association between APOE ϵ 4 genotype and cerebrospinal fluid tau in women when compared with men. It is possible that sex differences may thus influence tau propagation

This is an open access article under the terms of the Creative Commons Attribution-NonCommercial License, which permits use, distribution and reproduction in any medium, provided the original work is properly cited and is not used for commercial purposes.

© 2020 The Authors. *Alzheimer's & Dementia: Diagnosis, Assessment & Disease Monitoring* published by Wiley Periodicals, Inc. on behalf of the Alzheimer's Association.

pathways. If there are sex-specific differences in tau propagation, this would lead to differential regional tau accumulations.

The brain can be modeled as a network of functionally,¹⁹ structurally,²⁰ and metabolically²¹ connected regions. We applied a graph theoretical approach to regional [¹⁸F]flortaucipir positron emission tomography (PET) signals to examine tau propagation pathways by generating networks of brain regions with correlated tau signals.⁸ Several network metrics were used to characterize the architecture or topology of the tau-based networks and determine how they mirror the Braak staging. Subsequently, we used these metrics to test for differences in network topology between men and women across diagnostic groups. We hypothesized that these differences may explain sex differences in tau burden and contribute to sex differences in the prevalence of AD.

2 | METHODS

2.1 | Study population

Data were obtained from the Alzheimer's Disease Neuroimaging Initiative (ADNI) database (adni.loni.usc.edu). This study was approved by the Institutional Review Board of Vanderbilt University Medical Center (IRB#181429). ADNI was launched in 2003 as a public-private partnership, led by Principal Investigator Michael W. Weiner, MD. Demographic, clinical, and imaging data for this study were collected from 462 ADNI subjects²² including clinically normal with and without subjective cognitive decline (CN ± SCD; 123 male and 178 female) and mild cognitive impairment patients, including early and late mild cognitive impairment (MCI; 101 male and 59 female). We chose all subjects who had tau scans at the time of download. Other data included age, cognitive performance, APOE ε4 status, and Aβ-positivity status. Subjects' data and the associated *p*-values for between-group differences are summarized in Table 1. In both CN and MCI groups, women were significantly younger than men. The CN-to-MCI decline in Mini-Mental Status Examination (MMSE) scores was significant for both men and women. MCI women had a significantly higher number of APOE ε4 carriers than CN women. In addition, MCI women had a higher number of Aβ-positive scans than CN women. However, this difference was only marginally significant (*p* = .06).

2.2 | Data acquisition and pre-processing

All ADNI [¹⁸F]flortaucipir scans were acquired at participating sites following the standardized ADNI protocol (adni.loni.usc.edu) for PET imaging. Briefly, an injection of 370 MBq ± 10% of radiotracer was followed by a 30-minute (6 × 5 minute frames) PET acquisition starting at 75-to-105 minutes after the injection of [¹⁸F]flortaucipir. The temporal frames were uploaded from each ADNI site to the USC's Laboratory of Neuroimaging ADNI database (LONI) where they were coregistered, averaged, and smoothed to obtain an isotropic resolution of 8 mm full width at half maximum (FWHM). Each subject's native-space MRI scan

RESEARCH IN CONTEXT

1. Systematic review: We reviewed the literature using traditional resources including PubMed, Google Scholar, and conference presentations. Sex-specific differences in brain-wide tau propagation are not fully understood. We examined networks of tau connectivity between brain regions based on correlations of their tau-positron emission tomography (PET) signal to evaluate sex-specific differences in brain-wide tau propagation.
2. Interpretation: Network characteristics in women may favor an accelerated brain-wide tau spread leading to higher tau burden in women than men, with implications for the greater female preponderance in Alzheimer's disease (AD) diagnosis.
3. Future directions: Future studies should explore other biological and genetic factors that may influence the sex-based differences in tau propagation.

was segmented and parcellated to 62 cortical and subcortical regions by LONI, which uses FreeSurfer (version 5.3.0) for the MPRAGE image segmentation and parcellation and calculates the mean flortaucipir uptake values from the coregistered PET scans. Table 2 provides a list of these regions and their corresponding assignment to the Braak stages I to VI. The PET uptake values were also corrected by the LONI team for partial volume effect using the Geometric Transfer Matrix (GTM) approach.²³ The partial volume corrected standardized uptake value ratios (SUVRs) from these regions, and several FreeSurfer-based reference regions were downloaded from the ADNI archive. Although the downloaded uptake values are intensity normalized (ie, SUVR), ADNI recommends users to conduct an additional intensity normalization with one of their FreeSurfer-defined reference regions. We selected the inferior cerebellar gray matter uptake reference region to reduce the influence of dorsal cerebellar off-target binding of flortaucipir. The template for the inferior cerebellar grey matter and flortaucipir implementation has been described by Diedrichsen²⁴ and implemented for flortaucipir reference region by Baker et al.²⁵

2.3 | Network generation and analysis

Using MATLAB 2018 (MathWorks, Inc., Natick, MA), networks of tau-connected brain regions (represented as nodes in a network model) were constructed by calculating the Pearson's correlation matrix of regional PET SUVRs across subjects similar to previous approaches.⁸ Each matrix element represents the correlation between two regions' SUVR values (represented as edges in a network model) across subjects with a value between 0 and 1.

Nodes and edges associated with each group were imported into Gephi (version 0.9.2)²⁶ to generate each group's tau-connectivity

TABLE 1 Subject characteristics by sex and clinical diagnosis group and pairwise comparison between groups

Variables	CN-women N = 179	CN-men N = 123	MCI-women N = 59	MCI-men N = 101
Age (years) (mean ± SD)	74 ± 7	77 ± 8	73 ± 8	76 ± 7
APOE ε4 carriers (%)	56 (32%)	34 (28%)	31 (53%)	37 (37%)
MMSE (mean ± SD)	29.1 ± 1.3	28.8 ± 1.5	26.6 ± 3.8	27.1 ± 3.8
Aβ positivity (%)	67 (38%)	47 (38%)	31 (53%)	47 (47%)
Pairwise comparison of between groups				
	CN-men vs. CN-women	MCI-men versus MCI- women	CN-men versus MCI-men	CN-women vs. MCI- women
Age	0.001*	0.02*	0.85	0.78
APOE ε4 carriers	0.54	0.08	0.22	0.01*
MMSE	0.053	0.15	<0.001*	<0.001*
Aβ positivity	0.97	0.57	0.28	0.06

p-value significance codes: 0 '**' .05.

APOE ε4, apolipoprotein E ε4 allele; Aβ, amyloid beta; CN, clinically normal; MCI, mild cognitive impairment; MMSE, Mini-Mental State Examination.

TABLE 2 Brain regions used for the construction of tau-based networks (columns 1, 3) and their associated Braak staging (columns 2, 4)

Region (left, right)	Braak stage	Region (left, right)	Braak stage
Entorhinal (L,R)	I	Medial orbitofrontal (L,R)	V
Hippocampus (L,R)	II	Superior temporal (L,R)	V
Parahippocampus (L,R)	III	Superior parietal (L,R)	V
Fusiform gyrus (L,R)	III	Precuneus (L,R)	V
Lingual gyrus (L,R)	III	Banks of superior temporal sulcus (L,R)	V
Amygdala (L,R)	III	Nucleus accumbens (L,R)	V
Middle temporal (L,R)	IV	Pars opercularis (L,R)	V
Caudal anterior cingulate (L,R)	IV	Lateral occipital (L,R)	V
Rostral anterior cingulate (L,R)	IV	Parietal supramarginal (L,R)	V
Posterior cingulate (L,R)	IV	Inferior parietal (L,R)	V
Isthmus cingulate (L,R)	IV	Pericalcarine cortex (L,R)	VI
Insular cortex (L,R)	IV	Precentral gyrus (L,R)	VI
Inferior temporal (L,R)	IV	Postcentral gyrus (L,R)	VI
Temporal pole (L,R)	IV	Paracentral lobule (L,R)	VI
Superior frontal (L,R)	V	Cuneus (L,R)	VI
Rostral middle frontal	V		

Regions from left and right hemispheres were included as separate network nodes.

network. Initially we had chosen a fixed cutoff threshold applied to the correlation matrices from all four groups to reduce the number of edges by eliminating those with low correlations. This caused the networks to have differing densities, which would make graph theory properties difficult to compare between networks. To address this issue, we determined for each individual network the highest cutoff for the SUVR correlation values where the network was fully connected (matched thresholds). All the graph metrics were reported at matched thresholds.

Multiple measures were derived from these networks. One common approach is to decompose the networks into subunits known as modules or communities, which are sets of regions more densely connected with each other than with the rest of regions in the network. We used the Louvain algorithm²⁷ to detect network communities. We ran the Louvain algorithm with Gephi's default resolution value, which is set to 1. The same resolution was applied to all four networks. We found that this default resolution worked best in terms of unraveling the Braak staging in the community parcellation of tau networks by partitioning

brain regions into pathologically meaningful communities. Selecting a higher resolution (finer partitioning), would divide the networks into a large number of small communities typically consisting of individual regions and their contralateral counterparts.

Connections between different communities occur through nodes with high betweenness centrality (BC). High BC nodes can be thought of as regions that influence connections between different communities (bridging nodes). In the context of tau networks, high BC nodes may present regions that could facilitate the spread of tau across different communities. Other network measures included the weighted degree (WD), a measure of the number and strength of direct connections of each node (from 0.7 to 1), and the closeness centrality (CC), a measure of a node's centrality in the network, where a higher nodal CC indicates that a node is closer to all other nodes (less intermediate nodes). These centrality measures fall within two major categories, radial and medial measures.²⁸ Radial measures (eg, WD) assess connections that emanate from or terminate at a given node, whereas medial measures (eg, BC) assess the number of walks (or pathways) that pass through a given node. The Yifan Hu²⁹ multilevel graph algorithm was implemented to visualize the networks in a way that the PET-based correlations between the nodes were encapsulated.

2.4 | Statistical analysis

We used the R Statistical Software version 3.5.3 (R Foundation for Statistical Computing, Vienna, Austria) for all analyses. We tested for between-group difference in MMSE, age, APOE $\epsilon 4$ status, and A β status. The associated *p*-values for between-group differences were calculated using the Wilcoxon rank-sum test for MMSE and age and the χ^2 test for APOE and A β variables (Table 1). Pairwise group differences in CC and WD between different groups were also assessed with the Wilcoxon rank-sum test. The nodal BC values of each group were binned and displayed as histograms and their 95th percentile values were calculated as a measure of their tail-heaviness (more regions with high BC) of the distribution. In addition to the graph metrics, non-parametric Wilcoxon rank-sum tests were used for simple pairwise group comparisons (CN-male, CN-female, MCI-male, MCI-female) of [¹⁸F]Flortaucipir SUVR values within Braak I, Braak II, Braak III-IV, and Braak V-VI regions without adjusting for any other variable. Then a series of linear regressions were conducted to examine the associations of tau SUVR values with sex while including age, diagnostic group, APOE $\epsilon 4$ status, and A β status as covariates. The A β positivity of each PET scan is determined by the LONI, which utilizes a summary region of interest (ROI) consisting of four cortical regions and calculates the normalized weighted means of these regions by using the whole cerebellum as reference region. LONI uses a threshold of 1.1 on all florbetapir PET scans to determine the A β positivity and 1.08 for A β -PET scans that were conducted with florbetaben. Two additional models (model 2 and model 3) were used to assess the interactions between sex and age as well as between sex and diagnostic group for predicting the SUVR values. We performed the Bonferroni correction

(*p* = .05/4) to adjust for multiple comparisons across different Braak-stage regions.

3 | RESULTS

3.1 | Network structure and community detection

Each tau network consists of 62 nodes (brain regions) connected by edges. Figure 1 shows the tau-based networks in CN-male, CN-female, MCI-male, and MCI-female groups. The color of the node represents the designated community (module) defined as a group of regions with their tau SUVR values being more strongly correlated with each other than with the rest of the network. The locations of the nodes in the network are not random but determined by the strength of their PET SUVR correlations. The visualization algorithm (Yifan Hu algorithm) that calculates the nodes' positions within the network does not have any information about their anatomical locations or any other type of structural/functional connectivity associated with these ROIs. The positions of the individual nodes in the network are purely based on PET signal correlations and do not have to map to their ROI locations in brain or be consistent across the groups. ROIs that have higher PET SUVR correlations with each other than with the rest of the ROIs congregate with each other within the realm of the network as communities. These communities are depicted with different colors in Figure 1. Regions associated with early Braak stages congregate together in the lower left corner of the network (community depicted with color black). Moving from the lower left to the upper right corner of the network, the early stage Braak regions start to merge with the mid-stage Braak regions and then the mid-stage Braak regions start to merge with the late-stage Braak regions. In summary, the spatial arrangement of these communities (calculated from cross-sectional PET images) closely resembled the temporal progression of tau across the Braak stages.

For the CN-male network, the Louvain algorithm detected three main communities. The majority of nodes within the first community were Braak stage I-IV regions (73%), whereas most nodes within the second community were Braak stage V regions (65%) and all of the nodes within the third community were associated with late-stage tauopathy (40% Braak V and 60% Braak VI).

The networks in MCI-male and CN-female groups consisted of four major communities. In these two subject groups, the (primarily) mid-stage Braak regions were separated by the hemispheric locations of the nodes into two distinct communities (depicted by two different colors for left and right hemispheres).

The MCI-female network had only two main communities (meaning lower modularity). These communities included the early to mid-stage Braak regions (community one) and mid- to late-stage Braak regions (community two). Table 3 lists the Braak stages identified in the decomposed communities (regions more densely connected with each other than with the rest of the network) in CN-male, CN-female, MCI-male, and MCI-female groups.

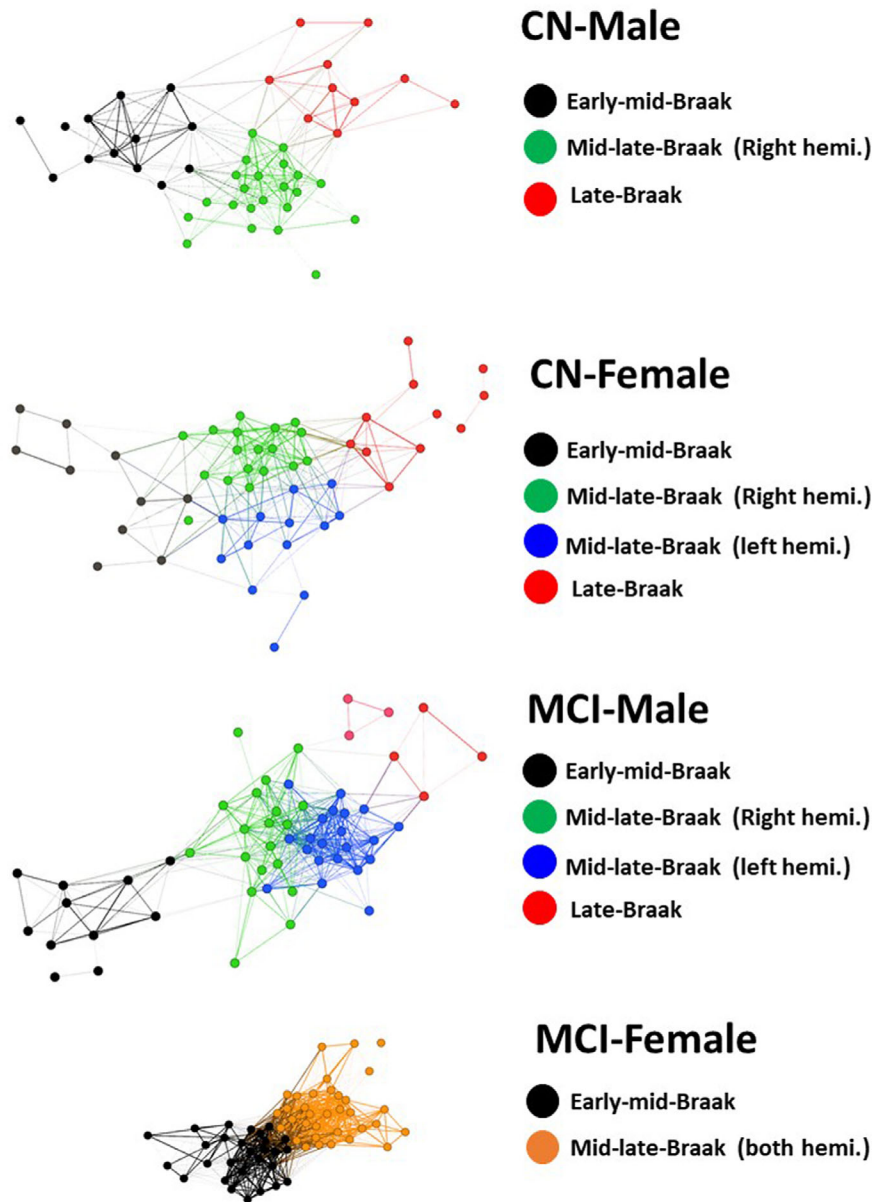


FIGURE 1 (Tau-based networks in four subject groups): Each node represents a brain region. The position of each node within the network is determined based on the strength of its PET SUVR correlations with other nodes. Regions that have higher PET correlations with each other than with the rest of the brain congregate to each other as communities depicted with different colors. CN, cognitively normal; hemi., hemisphere; MCI, mild cognitive impairment

Overall, the MCI women's network exhibited the lowest modularity (lowest Newman's Q) across a range of correlation thresholds and resolution parameter in Louvain's algorithm. The details of the modularity analysis are summarized in the supplement.

Across a range of explored thresholds (0.5 to 0.9), the CN-male group exhibited the lowest and the MCI-female group had the highest network densities (Figure 2A). The graph density indicates how close the calculated number of edges is to the maximum number of possible edges defined as $n*(n-1)/2$, with n being the number of nodes/regions. The minimum density at which the networks were fully connected were identified as 0.2 in CN-male, 0.22 (CN-female), 0.27 (MCI-male), and 0.33 in MCI-female. The highest cutoff values for correlation matrices

associated with these minimum densities were 0.68 (CN-male), 0.65 (CN-female), 0.70 (MCI-male), and 0.77 (MCI-female). All the subsequent graph metrics were calculated at minimum densities at which the associated networks were fully connected (matched thresholds) to enable comparison across networks with different densities.

3.2 | Network metrics

3.2.1 | Betweenness centrality (BC) in CN groups

Connections between different communities are influenced by nodes with high BC. At matched thresholds, the top 95th percentile value

TABLE 3 Braak —stages identified in the decomposed communities

Group	Decomposed community	SUVR (mean ± SD)	Braak stage (%)
CN-Male	Black	1.47 ± 0.31	I-IV (73)
			V (27)
	Green	1.47 ± 0.22	IV (35)
			V (65)
	Red	1.48 ± 0.21	V (40)
			VI (60)
CN-Female	Black	1.42 ± 0.46	I-IV (100)
	Blue (left hemisphere)	1.48 ± 0.28	III (19)
			IV (45)
			V (36)
	Green (right hemisphere)	1.51 ± 0.29	III (13)
			IV (27)
MCI-Male			V (60)
	Red	1.53 ± 0.27	V (50)
			VI (50)
	Black	1.61 ± 0.64	I-IV (82)
			V (18)
	Blue (left hemisphere)	1.60 ± 0.53	II (16)
MCI-Female			IV (42)
			V (42)
	Green (right hemisphere)	1.57 ± 0.50	II (16)
			IV (42)
			V (42)
	Red	1.46 ± 0.24	IV-V (28)
MCI-Female			VI (72)
	Black	1.78 ± 0.75	I-IV (78)
			V (22)
	Orange	1.74 ± 0.77	III-IV (18)
			V-VI (82)

CN, Clinically normal; MCI, mild cognitive impairment; SUVr, standardized uptake value ratio.

of the BC distribution (across 62 nodes) was 0.06 in the CN-male network and 0.07 in the CN-female network. In the CN-male network, the left parahippocampus was among the regions with the highest BC (BC = 0.12) and served as a bridging node between entorhinal cortex and other regions, most notably those within temporal and parietal lobes. The left supramarginal gyrus was the second high-BC node (BC = 0.11), which served as a bridging node between the early stage tau, mid-stage tau, and late-stage communities. In the CN-female network, the right parahippocampus (BC = 0.06) connected the entorhinal cortex with temporoparietal regions. The right fusiform gyrus (BC = 0.11) and right lingual gyrus (BC = 0.08) were identified as other nodes with the highest BCs. Only a marginally significant pairwise BC difference were detected between men and women in the CN group ($p = .1$).

3.2.2 | Betweenness centrality (BC) in MCI groups

At matched thresholds, the 95th percentile value of the BC distribution (across 62 nodes) was 0.09 in MCI-male network and 0.05 in the MCI-female network. In the MCI-male network, the left amygdala (BC = 0.09), right parahippocampus (BC = 0.09), left insular cortex (BC = 0.094), and right superior parietal (BC = 0.1) were identified as regions with the highest BC. The BC distribution of the MCI-female network was distinct from the other groups by showing a large number of low and intermediate BC values, with right parahippocampi and left amygdala being among the regions ranked within the top 95th percentile BCs. The histograms of the BC distributions and their associated 95th percentiles at matched thresholds are presented in Figure 2B.

3.2.3 | Closeness centrality (CC)

CC is calculated as the sum of the length of the shortest paths (minimum number of intermediate nodes) between a node and all other nodes in the network. The more central a node is, the closer it is to all other nodes, which may influence the efficiency of tau spread across these regions. Figure 2C shows the CC box plots in CN-male, CN-female, MCI-male, and MCI-female at their matched thresholds (highest SUVr correlation cutoffs for fully connected networks across). The MCI-female network had the highest median CC (0.57 ± 0.14). Significant pairwise CC differences were detected between MCI-male and MCI-female ($p < .001$) and CN-female and MCI-female ($p = .007$).

3.2.4 | Weighted degree (WD)

WD indicates the number and strength of connections between a node and other nodes. Figure 2D presents the box plots of the WDs in the four networks at matched thresholds. The median network WD value increased from CN to MCI, with the MCI-female network having the highest average WD (19 ± 9). At matched threshold, significant pairwise differences were detected between MCI and CN in both male ($p = .003$) and female ($p < .001$) participants as well as between the sexes in CN groups ($p = .025$) and MCI groups ($p < .001$).

The computed graph metrics (WD, CC, and BC) from the CN-men, CN-women, MCI-men, and MCI-women networks were compared against their null models (randomized versions of the original networks) to ensure that these graph metric values would not be explained on the basis of chance alone.^{30,31} We generated null models of each network using the Maslov-Sneppen rewiring algorithm.³⁰ The graph metrics WD, CC, and BC (the top 95th percentile of the BC distribution) of the original networks and their null models were compared by using the Wilcoxon rank-sum test. Across all four networks, we found significant differences in WD ($p < .001$) and CC ($p < .01$) between original networks and their null models. In CN-female, MCI-male, and MCI-female, we found significant differences ($p < .033$) in BC between original networks and their null models.

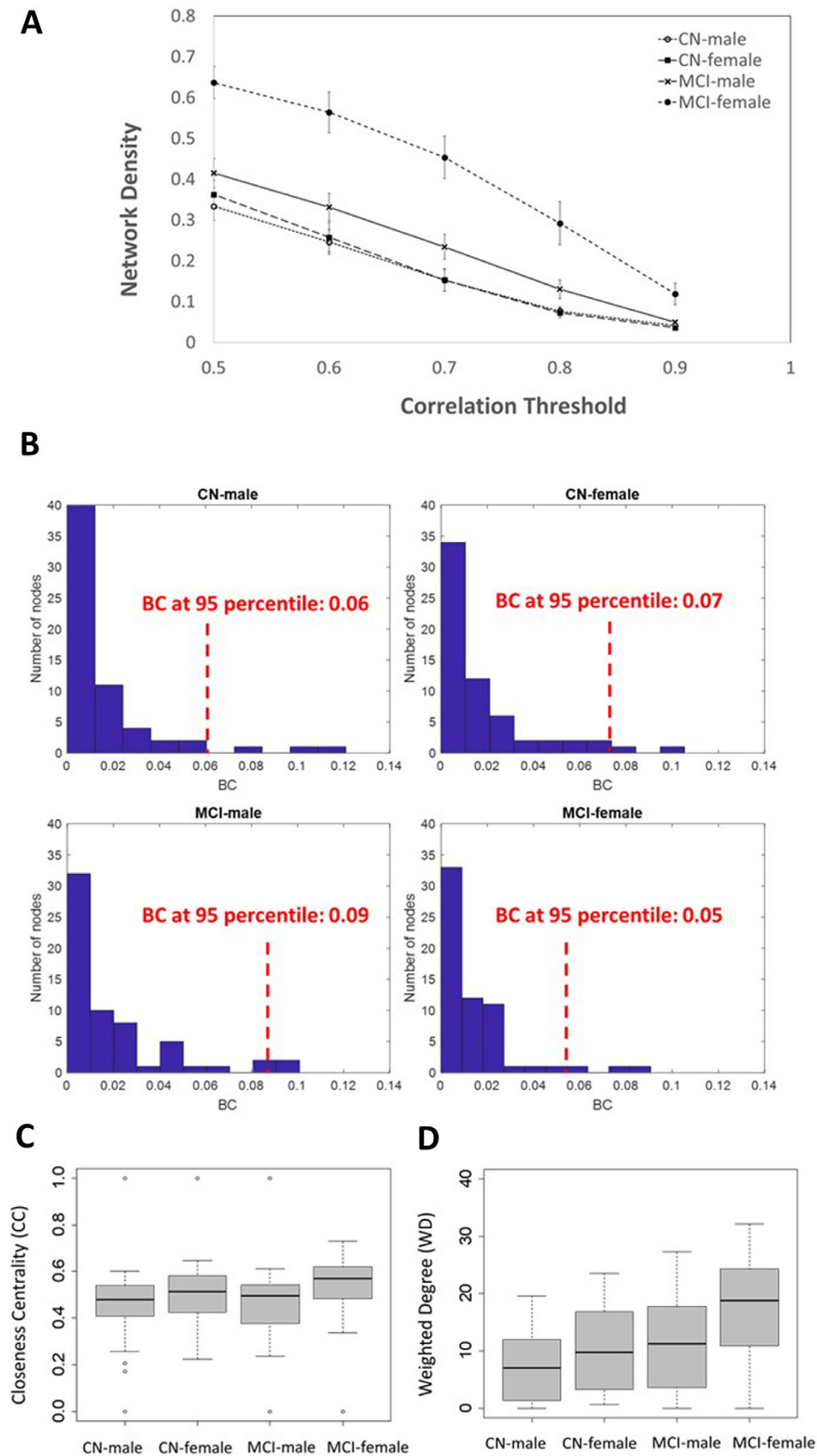


FIGURE 2 Network densities as a function of correlation threshold (A); the betweenness centrality (BC) histograms in CN-male, CN-female, MCI-male, and MCI-female with the associated 95th percentile values of their distributions at matched threshold (B); and the boxplots of closeness centrality (CC) (C) and weighted degree (WD) (D) in CN-male, CN-female, MCI-male, and MCI-female groups at matched thresholds

3.3 | Sex-specific differences in regional tau burden

Using simple group comparisons without adjusting for age, we detected 30% increase ($p < .001$) in Braak I SUVR, 23% in Braak III-IV SUVR ($p = .001$), and 16% increase in Braak V-VI SUVR ($p = .002$) from CN to MCI in women. A lower magnitude of increased SUVR between CN-MCI was observed in men. Here we detected 23% increase ($p < .001$) in Braak I SUVR, 10% in Braak III-IV SUVR ($p = .01$), and 7% increase in Braak V-VI SUVR ($p = .02$) from CN to MCI. In addition, we found significantly higher SUVR values for women as compared to men both at CN (Braak V-VI) and MCI stages (Braak III-VII).

The linear regression analysis showed that, across all Braak regions, higher SUVR values were associated with sex while accounting for age, clinical diagnostic group, *APOE* $\epsilon 4$ status, and *A β* status. Significant two-way interactions were found between diagnostic group and sex in predicting tau SUVR values in Braak III-IV and Braak V-VI regions. For other regions, these interactions were marginally significant (Braak II) or non-significant (Braak I). We did not detect any interactions between age and sex. Table 4 shows the summary of the statistical analyses.

4 | DISCUSSION

The tau network topology of women with MCI looked different than the other three groups. Women with MCI stood out as having the highest network density, characterized by a large number of direct connections (highest WD and CC) between individual brain regions in co-occurrence with increased brain-wide tau burden. The WD is a commonly used network centrality measure,³² and regions with high WD have more connections to other regions. In the context of tau propagation, high WD may be interpreted as a region that can rapidly encourage the spread of its tauopathy to all other regions that are directly connected with it (regions within the same community).

The more widespread increase of tau burden from CN-MCI in women than men (see changes in Braak V-VI SUVR) may be explained by comparing the MCI-female's BC distribution with the CN-female's BC distribution where several key regions served as bridging nodes between mid-late Braak-stage communities. These high-BC regions, located at the tail end of the BC histograms, may play an early role in the tau spread across wider brain regions (between different communities). We hypothesize that the presence of several high-BC nodes in the CN-female group may favor an accelerated brain-wide tau spread in women, subsequently leading to higher neocortical [¹⁸F]flortaucipir SUVR values, particularly at MCI stages (Table 4). The dense MCI-female network architecture is potentially a downstream effect of the accelerated tau spread, which subsequently modifies the network community structure by reducing the modularity (communities merge together). These changes in the network architecture consequently reduce the BC values of the previously high-BC nodes because these regions are no longer needed to facilitate the spread of tau across different communities. The similarity in the overall BC distributions between CN-female and MCI-male networks may indicate that the

topological changes of tau-based networks in men occur later than those in women. It remains to be determined whether the MCI-male group will eventually (perhaps at a later AD stage) exhibit a dense network of brain-wide tau connections similar to that observed in the MCI-female network. For this study, we used standard centrality measures that were available in our software package. However, it is possible that tau spread would follow a diffusion process. Therefore, we consider using diffusion-based counterparts to closeness centrality and betweenness centrality in future studies, as it may offer novel insights into tau propagation pathways. The relationship between a node's centrality and its flortaucipir SUVR value is not straightforward. For instance, we (and others, eg, Buckley et al.¹⁷) have observed high tau SUVR in the entorhinal cortex (also see Table 4), which is a region with relatively low centrality located at lower right corner of the network. Moreover, the PET network is obtained from population-based correlations (PET regional correlations across different subjects instead of time series). This means that each node within a network is associated with a single graph metric value (eg, WD) whereas the node's SUVR value varies across the subjects. Taken together, the associations between centrality measures and tau SUVR requires a more comprehensive analysis, which will be the objective of future work.

The sex-based differences in the tau network topology may indicate differences in anatomical and functional pathways and the strength of their associated connectivities that can contribute to sex-related vulnerability for AD. Previous studies have shown that women have structural³³ and functional³⁴ network characteristics that are different from those in men. Neuroimaging studies have demonstrated a modular organization of the brain function and structure, defined as the ability to segregate the brain connectivity patterns into distinct sub-networks. The modularity emerges early in life and refines during adolescence where the structural and functional modules become more segregated, presumably to develop the executive functioning performance in youth.³⁵ Measuring the diffusion-based structural connectome of children and adolescents, Ingahlalikar and colleagues³⁶ reported higher inter-modular structural connectivity in female than in male subjects. Using diffusion MRI data, a study by Tunc and colleagues³⁷ examined sex differences in the modularity of the structural connectome by implementing the Louvain algorithm, which was similar to our approach with tau networks. In their study, men showed significantly higher modularity than women, which corroborates with the modularity findings of our study with tau-PET networks. Moreover, a resting-state functional magnetic resonance imaging (fMRI) connectivity study with graph analysis by Zhang et al.³⁸ reported higher local efficiency and stronger clustering coefficient in men compared to women. These findings were in close agreement with Ingahlalikar's diffusion tensor imaging -based graph analysis, which found a significantly higher participation coefficient in women than in men. Low participation coefficient (nodes' preference to connect within their communities) and high clustering coefficient (nodes' tendency to cluster together) in men suggest that their functional/structural brain communities exhibit more segregation, whereas women have higher integration between these communities. Higher integration in women may favor a faster propagation of tau, leading to our observed higher (and

TABLE 4 Group comparisons of Braak I-VI SUVR values by sex and diagnosis and regression analysis

Group comparisons (by sex)			
Regions	Women SUVR	Men SUVR	p value
Women versus men in CN			
Braak I	1.69 ± 0.39	1.61 ± 0.36	.10
Braak II	1.34 ± 0.22	1.34 ± 0.21	.61
Braak III-IV	1.48 ± 0.20	1.45 ± 0.19	.22
Braak V-VI	1.54 ± 0.17	1.48 ± 0.15	.001*
Women versus men in MCI			
Braak I	2.19 ± 0.89	1.98 ± 0.85	.16
Braak II	1.66 ± 0.52	1.54 ± 0.45	.13
Braak III-IV	1.82 ± 0.70	1.59 ± 0.40	.008*
Braak V-VI	1.79 ± 0.57	1.59 ± 0.32	<.001*
Group comparisons (by diagnosis)			
CN versus MCI in men	CN SUVR	MCI SUVR	p value
Braak I	1.61 ± 0.36	1.98 ± 0.85	<.001*
Braak II	1.34 ± 0.21	1.54 ± 0.45	.004*
Braak III-IV	1.45 ± 0.19	1.59 ± 0.40	.01*
Braak V-VI	1.48 ± 0.15	1.59 ± 0.32	.02
CN versus MCI in women			
Braak I	1.69 ± 0.39	2.19 ± 0.89	<.001*
Braak II	1.34 ± 0.22	1.66 ± 0.52	<.001*
Braak III-IV	1.48 ± 0.20	1.82 ± 0.70	<.001*
Braak V-VI	1.54 ± 0.17	1.79 ± 0.57	<.001*
Regression Analyses			
Model 1: tau SUVR ~ Sex + Age + DX + APOE + Aβ	β (95% CI) for Sex		p value for Sex
Region			
Braak I	0.13 (0.08, 0.19)		.016
Braak II	0.06 (0.03, 0.09)		.056
Braak III-IV	0.08 (0.05, 0.12)		.011*
Braak V-VI	0.10 (0.07, 0.13)		<.001*
Model 2: tau SUVR ~ Sex*DX + Age + APOE + Aβ	β (for sex*DX)		p-value (for sex*DX)
Region			
Braak I	0.04(-0.002, 0.08)		.35
Braak II	0.04(0.02, 0.06)		.07
Braak III-IV	0.07(0.04, 0.09)		.005*
Braak V-VI	0.06(0.04, 0.08)		.004*
Model 3: tau SUVR ~ Sex*Age + DX + APOE + Aβ	β (for sex*age)		p-value (for sex*age)
Braak I	0.004 (-0.003, 0.011)		0.54
Braak II	0.003(-0.007, 0.007)		0.41
Braak III-IV	0.0007(-0.004, 0.005)		0.87
Braak V-VI	0.001(-0.002, 0.005)		0.70

Significance codes (Bonferroni-adjusted p -value .05/4 = 0.0125): 0 "***" 0.0125.

CN, clinically normal; DX, clinical diagnosis group; MC, mild cognitive impairment; SUVR, standardized uptake value ratio.

more widespread) SUVR values for women in Braak V-V1 (CN) and Braak III-VI (MCI).

Although sex difference in the brain connectome is present at young ages, the developmental trajectory of sex-based differences as related

to aging and age-induced biological changes remains relatively unexplored. Compared to normal menopause, premature hormonal losses before menopause are associated with increased risk of cognitive impairment and dementia.³⁹ Although early postmenopausal women

with cognitive complaints show evidence of altered (functional) brain connectivity,⁴⁰ the associations between hormonal-related changes in the overall (structural and functional) brain connectome and progression of tau in normal and pathological aging is not clearly understood. Although we currently do not have access to specific medical information to delineate hormonal changes in ADNI (female) participants, future studies should explore relationships between tau propagation and the hormonal milieu occurring after menopause, including age at menopause and any use of hormonal supplementation. The brain is a major target for circulating gonadal steroids, and the change in hormone levels after menopause appears to have implications for cognitive functioning. A number of clinical and preclinical studies have linked hormones and cognition,⁴¹⁻⁴³ and it has been hypothesized that menopause has detrimental effects on cognition that are over and above the expected effects of normal aging. Although the neuroprotective actions of hormones, such as estrogen, are related mainly to A β production and clearance, some studies have shown that the phosphorylation sites in tau are influenced by hormones, including estrogen and progesterone.^{44,45} Studies of tau density and spread in the years after menopause could help clarify any potential effects of menopause on the sex differences seen in this study.

Women have a lifelong advantage in verbal memory,⁴⁶⁻⁴⁹ which is the most frequently used domain to diagnose AD. Women's superior verbal memory skills may be a form of cognitive reserve and explain why women show higher and more widespread tau burden than men at comparable cognitive stages. Our tau SUVR findings are informed by a previous investigation by Sundermann and colleagues⁴⁷ showing evidence of better verbal memory in woman with amnesic MCI than men, despite similar levels of temporal lobe hypometabolism. Moreover, their observed sex differences in verbal memory was most evident at low to moderate neurodegeneration (none to moderate hypometabolism) but declined among individuals at advanced neurodegeneration, suggesting that verbal memory may represent a female-specific form of cognitive reserve, which helps women to withstand higher pathological insult (eg, higher tau burden) before becoming symptomatic and crossing thresholds for diagnoses of AD. Currently, relatively few ADNI AD subjects have tau scans. As the number of ADNI tau scans increases, future cross-sectional and longitudinal studies will include networks from other clinical diagnostic groups, including AD subjects, to determine whether the observed sex differences intensify over time and in AD.

Future studies should explore biological factors, such as differences in the timing of the menopause that may influence the sex-based differences in tau propagation. Such work could advance sex-specific risk-mitigation strategies including hormonal therapies, preventive interventions, and cognitive remediation. Our data support the findings of sex differences in dementia risk and previous reports of sex differences in tau accumulation. We further hypothesize that sex-specific differences in brain's functional, neuroanatomical, and pathological organization may map into differences at neurobehavioral and cognitive level, thus explaining differences in the prevalence of neurodegenerative disorders.

ACKNOWLEDGMENTS

Data collection and sharing for this project was funded by the ADNI (National Institutes of Health Grant U01 AG024904) and DOD ADNI (Department of Defense award number W81XWH-12-2-0012). ADNI is funded by the National Institute on Aging, the National Institute of Biomedical Imaging and Bioengineering, and through generous contributions from the following: AbbVie, Alzheimer's Association; Alzheimer's Drug Discovery Foundation; Araclon Biotech; BioClinica; Biogen; Bristol-Myers Squibb; CereSpir; Cogstate; Eisai; Elan Pharmaceuticals; Eli Lilly; EuroImmun; F. Hoffmann-La Roche & Genentech; Fujirebio; GE Healthcare; IXICO; Janssen Alzheimer Immunotherapy Research & Development; Johnson & Johnson Pharmaceutical Research & Development; Luminosity; Lundbeck; Merck & Co; MesoScale Diagnostics; NeuroRx Research; Neurotrack Technologies; Novartis Pharmaceuticals Corporation; Pfizer; Piramal Imaging; Servier; Takeda Pharmaceutical Company; and Transition Therapeutics. The Canadian Institutes of Health Research is providing funds to support ADNI clinical sites in Canada. Private sector contributions are facilitated by the Foundation for the National Institutes of Health (www.fnih.org). This project was supported by the National Institutes of Health (R01 EB009106 to S.S., K24 MH110598 to W.D.T., and R01 AG047992 to P.A.N.).

CONFLICTS OF INTEREST

Authors have no competing interests.

REFERENCES

1. Clavaguera F, Bolmont T, Crowther RA, et al. Transmission and spreading of tauopathy in transgenic mouse brain. *Nat Cell Biol*. 2009;11(7):909-913.
2. Frost B, Jacks RL, Diamond MI, Propagation of tau misfolding from the outside to the inside of a cell. *J Biol Chem*. 2009;284(19):12845-12852.
3. Hasegawa M, Molecular mechanisms in the pathogenesis of alzheimer's disease and tauopathies-prion-like seeded aggregation and phosphorylation. *Biomolecules*. 2016;6(2):24.
4. Holmes BB, Diamond MI, Prion-like properties of tau protein: the importance of extracellular tau as a therapeutic target. *J Biol Chem*. 2014;289(29):19855-19861.
5. Goedert M, Spillantini MG, Propagation of tau aggregates. *Molecular brain*. 2017;10(1):18-18.
6. Braak H, Braak E, Frequency of stages of Alzheimer-related lesions in different age categories. *Neurobiol Aging*. 1997;18(4):351-357.
7. Braak H, Del Tredici K, Spreading of tau pathology in sporadic alzheimer's disease along cortico-cortical top-down connections. *Cereb Cortex*. 2018;28(9):3372-3384.
8. Sepulcre J, Grothe MJ, d'Oleire Uquillas F, et al. Neurogenetic contributions to amyloid beta and tau spreading in the human cortex. *Nat Med*. 2018; 24(12):1910-1918.
9. Franzmeier N, Neitzel J, Rubinski A, et al. Functional brain architecture is associated with the rate of tau accumulation in Alzheimer's disease. *Nat Commun*. 2020; 11:347. <https://doi.org/10.1038/s41467-019-14159-1>.
10. Jacob W Vogel, Yasser Iturria-Medina, Olof T Strandberg, Ruben Smith, Alan C Evans, Oskar Hansson, Spread of pathological tau proteins through communicating neurons in human Alzheimer's disease, for the Alzheimer's Disease Neuroimaging Initiative, and the Swedish BioFinder Study bioRxiv 555821; <https://doi.org/10.1101/555821>

11. Hoenig MC, Bischof GN, Seemiller J, et al. Networks of tau distribution in Alzheimer's disease. *Brain*. 2018;141(2):568-581.
12. Mazure CM, Swendsen J. Sex differences in Alzheimer's disease and other dementias. *Lancet Neurol*. 2016;15(5):451-452.
13. Carter CL, Resnick EM, Mallampalli M, Kalbarczyk A. Sex and gender differences in Alzheimer's disease: recommendations for future research. *J Women's Health*. 2012;21(10):1018-1023.
14. Viña J, Lloret AC. Why women have more Alzheimer's disease than men: gender and mitochondrial toxicity of amyloid-beta peptide. *J Alzheimer's Dis: JAD*. 2010;20(suppl 2):527.
15. Plassman BL, Langa KM, Fisher GG, et al. Prevalence of dementia in the United States: the aging, demographics, and memory study. *Neuroepidemiology*. 2007;29(1-2):125-132.
16. Hebert LE, Weuve J, Scherr PA, Evans DA. Alzheimer disease in the United States (2010-2050) estimated using the 2010 census. *Neurology*. 2013;80(19):1778-1783.
17. Buckley RF, et al. Sex differences in the association of global amyloid and regional tau deposition measured by positron emission tomography in clinically normal older adults. *JAMA Neurol*. 2019;76(5):542-551. <https://doi.org/10.1001/jamaneurol.2018.4693>.
18. Hohman TJ, et al. Sex-specific association of apolipoprotein E with cerebrospinal fluid levels of tau. *JAMA Neurol*. 2018;75(8):989-998. <https://doi.org/10.1001/jamaneurol.2018.0821>.
19. Power JD, Cohen AL, Nelson SM, et al. Functional network organization of the human brain. *Neuron*. 2011;72(4):665-678.
20. Iturria-Medina Y, Canales-Rodríguez EJ, Melie-García L, et al. Characterizing brain anatomical connections using diffusion weighted MRI and graph theory. *Neuroimage*. 2007;36(3):645-660.
21. Huang S, Li J, Sun L, et al. Learning brain connectivity of Alzheimer's disease by sparse inverse covariance estimation. *Neuroimage*. 2010;50(3):935-949.
22. Petersen RC, Aisen PS, Beckett LA, et al. Alzheimer's Disease Neuroimaging Initiative (ADNI): clinical characterization. *Neurology*. 2010;74(3):201-209.
23. Rousset OG, Ma Y, Evans AC. Correction for partial volume effects in PET: principle and validation. *J Nucl Med*. 1998;39(5):904-911.
24. Diedrichsen J. A spatially unbiased atlas template of the human cerebellum. *Neuroimage*. 2006;33(1):127-138.
25. Baker SL, Maass A, Jagust WJ. Considerations and code for partial volume correcting [(18)F]-AV-1451 tau PET data. *Data Brief*. 2017;15:648-657.
26. Bastian M, Heymann S, Jacomy M. Gephi: an open source software for exploring and manipulating network. 2009. International AAAI Conference on Weblogs and Social Media.
27. Blondel VD, Guillaume JL, Lambiotte R, Lefebvre E. Fast unfolding of communities in large networks. *J Stat Mech: Theory Exp*. 2008;2008(10):P10008.
28. Borgatti SP, Everett MG. A Graph-theoretic perspective on centrality. *Social Networks*. 2006;28(4):466-484.
29. Hu Y. Algorithms for visualizing large networks. *Combinatorial Scientific Computing*. 2011;5(3):180-186.
30. Maslov S, Sneppen K. Specificity and stability in topology of protein networks. *Science*. 2002;296(5569):910.
31. Hanhijärvi S, Garriga GC, Puolamäki K. Randomization techniques for graphs. *Proceedings of the 2009 SIAM International Conference on Data Mining*. 2009:780-791.
32. Telesford QK, Simpson SL, Burdette JH, Hayasaka S, Laurienti PJ. The brain as a complex system: using network science as a tool for understanding the brain. *Brain Connect*. 2011;1(4):295-308.
33. Gong G, Rosa-Neto P, Carbonell F, Chen ZJ, He Y, Evans AC. Age- and gender-related differences in the cortical anatomical network. *J Neurosci*. 2009;29(50):15684-15693.
34. Tomasi D, Volkow ND. Gender differences in brain functional connectivity density. *Hum Brain Mapp*. 2012;33(4):849-860.
35. Baum GL, Ciric R, Roalf DR, et al. Modular segregation of structural brain networks supports the development of executive function in youth. *Curr Biol*. 2017;27(11):1561-1572.e8.
36. Ingalhalikar M, Smith A, Parker D, et al. Sex differences in the structural connectome of the human brain. *Proc Natl Acad Sci U S A*. 2014;111(2):823-828.
37. Tunç B, Solmaz B, Parker D, et al. Establishing a link between sex-related differences in the structural connectome and behaviour. *Philos Trans R Soc Lond B Biol Sci*. 2016;371(1688):20150111-20150111.
38. Zhang C, Cahill ND, Arbabshirani MR, White T, Baum SA, Michael AM. Sex and age effects of functional connectivity in early adulthood. *Brain Connect*. 2016;6(9):700-713.
39. Rocca WA, Bower JH, Maraganore DM, et al. Increased risk of cognitive impairment or dementia in women who underwent oophorectomy before menopause. *Neurology*. 2007;69(11):1074-1083.
40. Vega JN, Zurkovsky L, Albert K, et al. Altered brain connectivity in early postmenopausal women with subjective cognitive impairment. *Front Neurosci*. 2016;10:433-433.
41. Greendale GA, Huang M-H, Wight RG, et al. Effects of the menopause transition and hormone use on cognitive performance in midlife women. *Neurology*. 2009;72(21):1850-1857.
42. Newhouse P, Dumas J. Estrogen-cholinergic interactions: implications for cognitive aging. *Horm Behav*. 2015;74:173-185.
43. Dumas J, Hancur-Bucci C, Naylor M, Sites C, Newhouse P. Estrogen treatment effects on anticholinergic-induced cognitive dysfunction in normal postmenopausal women. *Neuropsychopharmacology*. 2006;31(9):2065-2078.
44. Shi H-R, Zhu L-Q, Wang S-H, et al. 17 β -estradiol attenuates glycogen synthase kinase-3 β activation and tau hyperphosphorylation in Akt-independent manner. *J Neural Transm*. 2008;115(6):879-888.
45. Alvarez-De-La-Rosa M, Silva I, Nilsen J, et al. Estradiol prevents neural tau hyperphosphorylation characteristic of Alzheimer's disease. *Ann N Y Acad Sci*. 2005;1052(1):210-224.
46. Kramer JH, Delis DC, Daniel M. Sex differences in verbal learning. *J Clin Psychol*. 1988;44(6):907-915.
47. Sundermann EE, Maki PM, Rubin LH, Lipton RB, Landau S, Biegon A, Alzheimer's Disease Neuroimaging Initiative. Female advantage in verbal memory: evidence of sex-specific cognitive reserve. *Neurology*. 2016;87(18):1916-1924.
48. Nebel RA, Aggarwal NT, Barnes LL, et al. Understanding the impact of sex and gender in Alzheimer's disease: a call to action. *Alzheimers Dement* 2018;14(9):1171-1183.
49. Asperholm M, Högman N, Rafi J, Herlitz A. What did you do yesterday? A meta-analysis of sex differences in episodic memory. *Psychol Bull*. 2019;145(8):785-821.

SUPPORTING INFORMATION

Additional supporting information may be found online in the Supporting Information section at the end of the article.

How to cite this article: Shokouhi S, Taylor WD, Albert K, Kang H, Newhouse PA, for The Alzheimer's Disease Neuroimaging Initiative. In vivo network models identify sex differences in the spread of tau pathology across the brain. *Alzheimer's Dement (Amst)*. 2020;12:e12016. <https://doi.org/10.1002/dad2.12016>